




Physical, mechanical, and radiation shielding studies: effects of glass network and ion valance states of Ti^{3+} and Mo^{5+} on TiO_2 -doped lead molybdenum borate glasses

Norah A. M. Alsaif¹ · S. Al-Omari² · Hanan Al-Ghamdi¹ · Y. S. Rammah³ · Z. Y. Khattari² 

Received: 6 July 2023 / Revised: 9 October 2023 / Accepted: 30 November 2023 / Published online: 6 December 2023
© The Author(s) under exclusive licence to Australian Ceramic Society 2023

Abstract

Effects on mechanical and γ -ray shielding competence of TiO_2 -based glasses of chemical composition: $30\text{PbO} \cdot 4\text{MoO}_3 \cdot (66 - z)\text{B}_2\text{O}_3 \cdot z\text{TiO}_2$ ($0.0 < z < 2.0$ mol%) was calculated in this report. The glass density was found to increase in the range of 4.650–4.696 g/cm^3 concurrent with a decline in the oxygen molar volume (OMV) from 10.633 to 10.547 cm^3/mol when $[\text{Ti}^{4+}]$ molar fraction is increased in the glass samples. The Gibbs free energy was found to be between 20.874 and 22.586 kJ/cm^3 and was found to be influenced by TiO_2 concentration in these glasses and on the valance states of Ti^{3+} and Mo^{5+} . The affinity of mass attenuation coefficient (MAC) values ($0.039 < \text{MAC} < 6.198$ g/cm^3) in the examined photon energy domain $0.015 < E < 15.0$ MeV has the following chronological sorting: $\text{MAC}_{\text{T0}} < \text{MAC}_{\text{T2}} < \text{MAC}_{\text{T4}} < \text{MAC}_{\text{T6}} < \text{MAC}_{\text{T8}} < \text{MAC}_{\text{T10}} < \text{MAC}_{\text{T15}} < \text{MAC}_{\text{T20}}$. The half-value-layer (HVL) trend of Mo-glasses was balanced against two standard RS-glass systems and discovered to possess a less γ -ray shielding competence as RS-(360, 520) or concrete. Also, we found that when the $[\text{Ti}^{3+}]/[\text{Mo}^{5+}]$ ratio exceeds 0.8 mol%, then both ions participate in the studied properties via de-polymerization of the glass network. These outcomes revealed that the safety effectiveness against radiation and physic-mechano-properties can be synchronized for diverse purposes.

Keywords Lead-molybdenum-boric glasses · Radiation shielding · Elastic moduli · MAC · Ion valance states

Introduction

Titanium dioxide is a unique inorganic compound with the chemical form TiO_2 [1]. This remarkable substance does not exist in its pure state in nature and is derived from naturally occurring ores that may contain trace amounts of other elements, depending on the ore's origin. These geological ores, which contain titanium minerals such as ilmenite, rutile, and anatase, are employed to synthesize pure TiO_2 [2, 3]. The intriguing TiO_2 is a polymorphic oxide that exhibits

three distinct crystal structures: monoclinic, tetragonal, and orthorhombic [3–6]. Fascinatingly, the primary function of TiO_2 is to serve as a pigment modifier [3–6]. This lustrous and brilliant solid-like colorless oxide is water-insoluble, while it may materialize as a black mineral. Its pigmentary properties have a vast variety of applications, which include paint, sunscreen, and/or food coloring. It is truly astonishing that it has been estimated that two-thirds of all pigments contain titanium dioxide [6]. Its splendor is unmatched, and since it was first produced on a large scale in 1916, TiO_2 has been extensively utilized in pallid pigment due to its resplendence and exceptionally high-refractive-index, which is only exceeded by other transparent glasses [7, 8]. It is interesting to notice that purity has a significant impact on the finished pigment is optical characteristics. In reality, the crystal structure can be disrupted by a few ppm of several metals, such as, but not limited to, chromium and Niobium, to the point that it can be identified during quality control [8]. Because TiO_2 is potent in its powdered type, it is utilized as a pigment assist in coatings, paints, plastics, inks, papers,

✉ Z. Y. Khattari
zkhattari@hu.edu.jo

¹ Department of Physics, College of Science, Princess Nourah Bint Abdulrahman University, P.O. Box 84428, 11671 Riyadh, Saudi Arabia

² Department of Physics, Faculty of Science, The Hashemite University, P. O. Box 330127, Zarqa 13133, Jordan

³ Department of Physics, Faculty of Science, Menoufia University, Shebin El-Koom 32511, Egypt

foods, dietary supplements, pharmaceuticals (i.e., pills and tablets), and even the majority of toothpastes [9, 10].

Glasses' employment in non-linear optical devices has been revolutionized by the addition of titanium oxide to them. This is because Ti^{4+} ions' unfilled d-orbitals greatly increase the non-linear polarizability [11]. These characteristics make them perfect for use in power limiters and ultra-fast switches [12, 13]. Moreover, it has been demonstrated that glasses containing TiO_2 have a negative non-linear refractive index, which causes radiation beams to self-focus within the substance. This indicates that these gadgets can function with less input power [14]. Fascinating fluorescence has also been seen in TiO_2 colored-glass materials, at significant oscillating power and broad band-widths. TiO_2 has been found to operate as a nucleating agent for crystallization, and it has been demonstrated that even modest amounts of titanium oxide in glass-based lead molybdenum borate materials can improve the shaping capacity and chemo-physico stability of these glass networks [15]. These findings have broad ramifications and could have a big impact on a lot of different sectors. Titanium oxide has long been regarded as a potent crystallization nucleating agent in the field of materials research. Furthermore, scientists have found that even modest amounts of TiO_2 in glass matrices can provide those improved glass-forming capabilities and chemical resistance [16]. Titanium-ions often present as a Ti^{4+} state and interact with the structural elements of TiO_4 , TiO_6 , or TiO_5 (made up of trigonal bi-pyramids) to create networks [16, 17]. The Ti^{3+} state of Ti-ions can also evolve in such glassy structures, according to various study studies [13, 18]. Regarding lead-borate-glass networks, the existence of two transition metals, more specifically, Mo and Ti-ions, is enticing since it is thought that their presence will have a significant impact on the glasses' physical characteristics [11–18]. Due to their propensity for catalysis, the molybdenum borate glasses have received the most attention of any of them [19, 20].

Molybdenum ions are known to occupy at least two steady valence states in systems like $PbO-B_2O_3$, namely molybdenum(V) and molybdenum(VI), in which they function as glass backbone structures catalysis, interspersing $[MoO_4^{2-}]-[BO_4]$ structure units. However, whether or not they can function as network modifiers also depends on their chemical weight fraction of the hosted structural networks [18–20]. Moreover, the addition of different metal oxides can act as a catalyst for significant modifications in structural and optical properties [21–24]. Alkali metals such as CaO , ZnO , MgO , and Na_2O might be useful modifiers to develop these characteristics. Moreover, when added to glass compositions, rare earth oxides such as Sm_2O_3 , Nb_2O_3 , Er_2O_3 , CeO_2 , Dy_2O_3 , and Gd_2O_3 cause obvious alteration in opto-electro properties [21–28]. The opto-physio and gamma-ray safety characteristics of glasses can also be significantly improved by the existence of HMO such PbO , WO_3 , Bi_2O_3 ,

and MoO_3 [24–27]. Depending on their presence in the glass composition, intermediate oxides like Y_2O_3 , Al_2O_3 , ZrO_2 , and Cr_2O_3 can function as either glass formers or glass modifiers [28]. Of interest, Prasad et al. delved into the impact of titanium oxide (TiO_2) on lead molybdenum borate glasses with an exploration of their dielectric, luminescence, optical absorption, luminescence, electron spin resonance, infrared spectra, and structural properties [29]. Also, different groups have studied the effect of incorporating the TiO_2 on various glass systems; see for instance [30]. The research showed that the density increased as TiO_2 content increased; also, the optical band gap and the reflective index increased up to a certain Ti ions addition and then gradually decreased. In the current effort, the unsettled effect of titanium oxide on the following glass chemical systems in the form: $30PbO + 4MoO_3 + (66 - z)B_2O_3 + zTiO_2$ ($0.0 < z < 2.0$ mol%). This research report will shed a light on the properties of neutron, gamma-ray radiation competence, and the physical, elastically, and mechanics of these glasses.

Materials and methods

Materials

Molybdenum-based glasses with promising catalytic properties may be tested for radiation protection for possible indoor or outdoor applications. Among them, Mo-PbO- B_2O_3 systems which exhibited two stable valence states in the glass network acting as structure stabilizer with $[MoO_4^{2-}]-$ structure-units flashing those of $[BO_4]-$ units and enhancing their electrical and dielectric properties to be used as a radiation shield with high interaction cross-section with incoming photon radiation. This research work deals with these types of glassy materials consisting of the different molar ratios by the addition of titanium oxide to it as a function of B_2O_3/TiO_2 molar ratio from 0 to 2 mol%. The samples were ground and optically polished. The final dimensions of the samples used for dielectric and optical studies were about $1 \times 1 \times 0.2$ cm³. The density d of the glasses was determined to an accuracy of 0.001 by the standard Archimedes' principle using o-xylene (99.99% pure) as the buoyant liquid. Table 1 displays the glass components in detail, and the sample coding has been done according to Ref. [29].

Theoretical and computational background

Geant4 Monte Carlo simulation

Due to obvious experimental difficulties in carrying out experiments due to financial restrictions or time management, scientists usually choose different approaches utilizing the well-known method of Monte Carlo simulations. Here,

Table 1 Chemical composition and the density of studied glass samples and the corresponding coding

| Sample code | PbO | MoO ₃ | B ₂ O ₃ | TiO ₂ | Density (g/cm ³) |
|-------------|-----|------------------|-------------------------------|------------------|------------------------------|
| T0 | 30 | 4 | 66 | 0 | 4.650 |
| T2 | 30 | 4 | 65.8 | 0.2 | 4.662 |
| T4 | 30 | 4 | 65.6 | 0.4 | 4.668 |
| T6 | 30 | 4 | 65.4 | 0.6 | 4.671 |
| T8 | 30 | 4 | 65.2 | 0.8 | 4.676 |
| T10 | 30 | 4 | 65.0 | 1.0 | 4.680 |
| T15 | 30 | 4 | 64.5 | 1.5 | 4.688 |
| T20 | 30 | 4 | 64.0 | 2.0 | 4.696 |

we have used Geant4 to simulate the shielding characteristics of the current samples. Among various numerical techniques, Geant4 simulation ranked as one of the most popular platforms to execute the Monte Carlo simulations in radiation-related research, nuclear physics, biomedical physics, and other science branches. For the radiation studies, Geant4 simulation provides a numerical pathway for studying the matter-radiation interactions that include a huge number of propagating particles, energies, and different nuclear models spanning an ample radius of energies from a few keV to MeV [31]. A Geant4 code has been used to model a high-purity germanium detector resembling shielding measurements to carry out the real-life experiments. Bioglass specimens were modeled as slabs in the current Geant4 model. The pre-defined detector geometry including shape, size, logical volume, physical volumes, material, sensitivity, and user limits has been set according to the internal codes of Geant4. Also, the material model follows the following procedure: describes the properties of atoms, the properties of elements, and the macroscopic properties of matter (i.e., density and state). Finally, build up from chemical molecules to a defined mixture with their own ratio of the components as a fractional mass and densities. Simulations were executed at incoming photon energies $150 \text{ keV} < E < 350 \text{ keV}$ at defined steps. An evacuated pathway is used in order to transmit the emitted photon intensity from the radioactive source to the detector. Then, the attenuated photon intensities were measured by placing the samples on the photon track between the source and the detector. The latter is achieved by employing Beer Lambert's law. Sample thickness was altered between 1.0 and 3.0 cm with 0.5 cm increment. A more detailed description of the simulation procedure and setup can be found in references [31].

XCOM program

The XCOM software [32, 33] is the oldest used web-based program to calculate the radiation mass attenuation coefficients of defined samples. XCOM program is a user-friendly

calculation program, and the input parameter specifications are quite flexible and easy to access via an internet database. In the XCOM program, each sample (i.e., shielding material) was defined by their elemental fractions. The mass attenuation coefficient of the investigated materials is then calculated by the XCOM program. This program does not perform the calculation of the other shielding parameters (i.e., LAC) and has to be calculated separately depending on the user's external software. Very recently, web-based programs have emerged to overcome these difficulties making it easy for the scientists to perform all of the shielding parameters via online platform [34].

Phys-X/SPD software

A user-friendly online photon shielding and dosimetry (PSD) software available at <https://phy-x.net/PSD> has been developed for the calculation of parameters relevant to shielding and dosimetry [34]. These parameters include linear and mass attenuation coefficients (LAC, MAC), half and tenth value layers (HVL, TVL), mean free path (MFP), effective atomic number and electron density (Z_{eff} , N_{eff}), and exposure buildup factors (EABF, EBF). The software can generate data on shielding parameters in the continuous energy region (1 keV–15 MeV). The software is freely available online after having registered into the Phy-X platform [34].

Physical properties

Using the Archimedes method and distilled water as a suspended solution, the density (ρ) of glass samples was evaluated at room temperature. Bulk glass samples were weighed twice, once in the air and again in distilled water, using calibrated five decimal point scales. This allowed calculating the value of glass density through the following equation:

$$\rho = \frac{w_a}{w_a - w_D} \times \rho_D \quad (1)$$

where w_a and w_D are the sample weight in the air and dibutyl-phthalate (DBP) and ρ_D is the DBP density. Units of density are g/cm^3 and an experimental accuracy of $\pm 0.01 \text{ g/cm}^3$. At a particular temperature and pressure, the molar volume, V_m , is the volume occupied by 1 mol of a substance from a chemical compound or chemical element [1, 35]. The following formula can be used to compute the molar volume (cm^3/mole) of each glass sample. In addition, the parameter OMV, which represents the volume of glass in 1 mol of oxygen, was evaluated from the equation shown below [1, 35]:

$$OMV = \left(\sum \frac{(x_i M_i)}{\rho} \right) \left(\frac{1}{\sum (x_i n_i)} \right) \quad (2)$$

where i is the number of oxygen atoms in each ingredient oxide, M_i is the molecular weight, and x_i is the molar fraction of each component i .

The oxygen packing density (OPD) values, which represent the arrangement of oxygen atoms in the glass system, were evaluated in terms of density and composition values by using the following formula:

$$OPD = 1000C \left(\frac{\rho}{M} \right) \quad (3)$$

Mechanical parameter basic relations: Makishima and Mackenzie theory

The elastic parameters of a material were evaluated by using Makishima-Mackenzie's theory [36–38]. This theory is based on the molecular weight (M), molar volume (V_m), and density (ρ) of the sample (see Table 1). Also, it depends on the measured dissociation energy which models the chemical bond strength between the oxide constituent (G_i) and the atomic packing factor (V_i) [36–38] for each oxide presented in the sample along with the calculated atomic packing density (V_t) defined as the ratio between the minimum theoretical volume occupied by the ions and the corresponding effective volume of glass. Then, the total dissociation energy of the glass mixture is readily determined according to the following equation:

$$G = \sum_i x_i G_i \quad (4)$$

where G_i and x_i are the dissociation energy and molar weight fraction of the i th component of the investigated glass, and the sum runs over all the glass mixture components. For poly-component glasses, the Young's modulus is expressed in terms of the packing density and the dissociation energy as

$$E = 2V_t G \quad (5)$$

where the atomic packing density is given in terms of the individual atomic packing factor of the oxide according to the following equation:

$$V_t = \frac{\rho}{M} \sum_i x_i V_i \quad (6)$$

The atomic packing factor (V_i) is obtained from the following equation for the oxide of the form A_xO_y :

$$V_i = N_A \frac{4\pi}{3} (XR_A^3 + YR_O^3) \quad (7)$$

In the last equation, each ion is modeled as a uniform sphere of ionic radius R_A and R_O for the metal and oxygen

respectively [36–38]. It is worth noting that the values of V_i and G_i can be readily obtained from references [39, 40]. Furthermore, other elastic moduli of the poly-component glasses (i.e., B , bulk modulus; S , shear modulus; L , longitudinal modulus; σ , Poisson's ratio; and H , micro-hardness) are calculated according to the following equations:

$$B = 1.2V_t E \quad (8)$$

$$S = \frac{3EB}{9B - E} \quad (9)$$

$$L = B + \frac{3}{4}S \quad (10)$$

$$\sigma = 0.5 - \frac{1}{7.2}V_t \quad (11)$$

$$H = \frac{1 - 2\sigma}{6(1 + \sigma)} \quad (12)$$

Shielding parameters basic relations

When a material of a thickness “ x ” is placed in the way of a radiant X-ray or gamma beam, the intensity of this beam is attenuated according to the exponential attenuation law (Beer Lambert's law)

$$\frac{I}{I_0} = e^{-\mu x} \quad (13)$$

where I_0 and I are the intensity before and after the attenuation respectively, x is sample thickness, and μ is the linear attenuation coefficient (LAC, μ in cm^{-1}) [32, 33]. The mass attenuation coefficient (MAC in cm^2/g) is a quantity that evaluates the probability of interaction of the photon with the material. MAC can be theoretically evaluated according to the mixture rule [32, 33]

$$MAC = \mu_m = \frac{\mu}{\rho} = \frac{1}{x} \ln \left(\frac{I_0}{I} \right) \quad (14)$$

The MAC values have been calculated using the above-mentioned web-based programs. The difference (Diff %) between the two calculated MAC values is evaluated according to the following equation

$$Diff(\%) = \frac{|(\mu_m)_{Phys} - (\mu_m)_{BUF}|}{(\mu_m)_{Phys}} \quad (15)$$

However, the HVT is a shielding parameter that introduces the thickness of the shielding material that is able to

diminish the incoming photon intensity to half of its value and can be calculated based on the LAC values according to the following equation [32, 33]

$$HVL = \frac{\ln(2)}{\mu} \quad (16)$$

The transmission factor (TF) is used to predict the ratio of γ -photon flux that can transmit a known thickness at any gamma photon energy and can be calculated as:

$$TF(\%) = \frac{I_0}{I} = e^{-\mu x} \quad (17)$$

Also, the radiation protection effectiveness (RPE) is defined as:

$$RPE = 1 - TF \quad (18)$$

Another important shielding property which may be derived from the basic physical quantities presented above is the removal cross-section (Σ_R) which is defined as the probability of a neutron collision in a specific homogenous material. The effective removal cross-section of the current glasses can be calculated based on the value of $\Sigma_{R/\rho}$ for each element that is used to prepare the glass mixture [32, 33]:

$$\Sigma_{R/\rho} = \sum_i w_i (\Sigma_{R/\rho})_i \text{ and} \quad (19)$$

$$\Sigma_R = \sum_i \rho_i (\Sigma_{R/\rho})_i$$

where ρ_i is the partial density of each element in the glass sample ($\text{g}\cdot\text{cm}^{-3}$), ρ is the total sample density ($\text{g}\cdot\text{cm}^{-3}$). In the current study, the effective removal cross-section was also determined using the new friendly Phy-X/PSD program [36].

Results and discussion

Physical features

Figure 1 depicts the molar volume (V_m) and density (ρ) of the investigated samples plotted against the Ti mol% on the left and right axes, respectively. The data reveals that the (V_m) decreased from 25.51 to 25.31 cm^3/mol , as evident from Table 2. Figure 1 and Table 2 also illustrate a rise in sample density from 4.65 to 4.696 g/cm^3 , as the Ti mol% increased within the glass network. The results indicate that the ρ of these glasses steadily improved as TiO_2 was introduced at the expense of B_2O_3 . This replacement affected both ρ and V_m , resulting in an increase and decrease in these intrinsic materialized quantities, respectively. This phenomenon can be ascribed to the replacement of the high molecular-weight

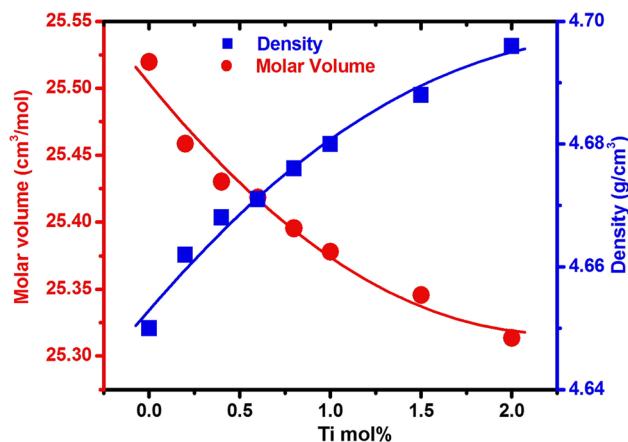


Fig. 1 Variation of density and molar volume as a function of Ti molar fraction present in glass samples. The lines are guide for the eyes and do not represent any empirical model

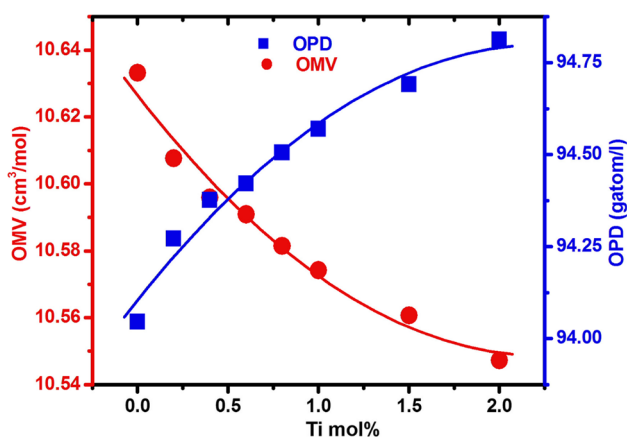
TiO_2 compound of 79.866 g/mol with the less molecular-weight B_2O_3 of 69.63 g/mol [38]. Furthermore, this substitution process caused an increase in NBO entities in these glassy networks, leading to an enhancement in glass density and oxygen packing density (OPD). This can be attributed to the Ti-atom functioning as a network stabilizer between the MoO_4^{2-} and the BO_4 primitive unit cell that evolves in the molecular structure of the compound [29]. Titanium atoms may also function as structure modifiers, as their concentrations or chemical composition are altered in the host network. Previous ESR research works in similar glassy networks, including Ti-ions, have confirmed the dual existence of octahedral coordinated Mo^{5+} ions mixed with deformed octahedrons, with probable tetragonal structures [39–41]. The glass systems contain PbO in their composition, which can cause further structural modification via oxygenation bridging between MoO_4 and PbO or BO_4 . Furthermore, the OMV and the corresponding OPD values are displayed in Table 2. The OMV was found to decrease with Ti mol%, while OPD increased (see Fig. 2). Figure 2 also shows a non-linear relationship between OMV and OPD as a function of Ti mol%. OPD values increased from 94.044 to 94.81 $\text{g}\cdot\text{atom}/\text{L}$, while OMV values decreased from 10.63 to 10.54 cm^3/mol (see Table 2). This could be due to the fact that the investigated glassy structures are more firmly packing the oxygen atoms as their chemical structures were tailored by bridging into the glass molecules TiO_2 compound [42–45].

Mechanical properties

When estimating the dissociation energy of TiO_2 glasses, the Makishima-Mackenzie model [36] typically takes into account the coordination changes, bond length, and packing volume [36, 37]. The estimated elastic modulus and

Table 2 Physical properties of the studied glass samples

| Sample code | Average molecular weight | Molar volume (cm ³ /mol) | Oxygen molar volume (cm ³ /mol) | Oxygen packing density (g atom/l) |
|-------------|--------------------------|-------------------------------------|--|-----------------------------------|
| T0 | 118.66668 | 25.51972 | 10.63322 | 94.04492 |
| T2 | 118.68717 | 25.45842 | 10.60768 | 94.27136 |
| T4 | 118.70766 | 25.43009 | 10.59587 | 94.37639 |
| T6 | 118.72815 | 25.41814 | 10.59089 | 94.42076 |
| T8 | 118.74864 | 25.39535 | 10.5814 | 94.50549 |
| T10 | 118.76914 | 25.37802 | 10.57418 | 94.57003 |
| T15 | 118.82036 | 25.34564 | 10.56068 | 94.69084 |
| T20 | 118.87159 | 25.31337 | 10.54724 | 94.81156 |

**Fig. 2** Oxygen molar volume (OMV) and oxygen packing density (OPD) as a function of Ti molar fraction presented in glass samples. The lines are guide for the eyes and do not represent any empirical model

Poisson's-ratio are summarized in Table 3. Here, through a discussion of the ν -parameter, we outline and go over the results of these elastic moduli. Since TiO_2 and B_2O_3 are competing for space in the glass networks' backbone net hardness despite having differing hardness, the observed non-monotonic trend in the ν -values may be the result of this [43–45]. A clear dependency on the combined effect of the Ti^{4+} ion concentration is also indicated by other moduli that

exhibit the same systemic behavior. Furthermore, for this glass series, there was no discernible variation in hardness (e.g., around 23.5 MPa) with $[\text{TiO}_2]$ molar proportion. In theory, the inter-atomic binding, the coordination number, and the directional-order-parameter in the primitive cells determine these elastic properties of such glasses [43–45]. It should be highlighted that these parameters are not known with absolute certainty because of blatant experimental roadblocks.

Radiation shielding properties

A 3D comparison graphic of the obtained MAC values calculated acquired from the online Phys-X software in the photon-energy range of $0.015 < E < 15.0$ MeV is shown in Fig. 3a. These data can be least-squared fitted using a decaying exponential function against the incoming photon energy. The figure also demonstrates that as the mol% concentrations of the component TiO_2 in the glasses rise, these values increase for the glasses encoded as T0-T_k , where $k \in [1, 19]$, respectively. These values at the lowest incoming photon energy $E = 0.015$ MeV are 60.019, 60.037, 60.055, 60.073, 60.091, 60.109, 60.153, and 60.198 cm²/g. The association between the ${}_{22}\text{Ti}^{48}$ element and the internal glass structure, which reflects the strength of the $\text{O}=\text{Ti}=\text{O}$ bonds and the matching $\text{O}=\text{Bi}-\text{O}-\text{Bi}=\text{O}$ bonding, can be used to explain this tendency. Such observable results were caused

Table 3 The mechanical parameters and elastic moduli of the investigated samples

| Sample code | ΣV_i (cm ³ /mol) | G (kJ/cm ³) | V_i (cm ³ /mol) | E (GPa) | B (GPa) | S (GPa) | L (GPa) | σ | H (GPa) |
|-------------|-------------------------------------|-------------------------|------------------------------|----------|----------|----------|----------|----------|---------|
| T0 | 18.0940 | 20.874 | 0.70902 | 29.60017 | 25.18453 | 11.34879 | 33.69612 | 0.40153 | 0.02342 |
| T2 | 18.0816 | 21.0452 | 0.71024 | 29.89429 | 25.47854 | 11.45860 | 34.07249 | 0.40136 | 0.02346 |
| T4 | 18.0692 | 21.2164 | 0.71054 | 30.15020 | 25.70751 | 11.55596 | 34.37448 | 0.40131 | 0.02347 |
| T6 | 18.0568 | 21.3876 | 0.71039 | 30.38707 | 25.90401 | 11.64712 | 34.63935 | 0.40133 | 0.02347 |
| T8 | 18.0444 | 21.5588 | 0.71054 | 30.63678 | 26.12239 | 11.74245 | 34.92923 | 0.40131 | 0.02347 |
| T10 | 18.0320 | 21.730 | 0.71054 | 30.88007 | 26.32983 | 11.83570 | 35.20660 | 0.40131 | 0.02347 |
| T15 | 18.0010 | 22.158 | 0.71022 | 31.47411 | 26.82425 | 12.06420 | 35.87240 | 0.40136 | 0.02346 |
| T20 | 17.9700 | 22.586 | 0.70990 | 32.06760 | 27.31775 | 12.29252 | 36.53714 | 0.40140 | 0.02345 |

Fig. 3 **a** MAC in the energy range $0.015 < E < 15$ MeV. **b** A comparison of the MAC values between XCOM data base and the online Phys-X program for the sample encoded as T6

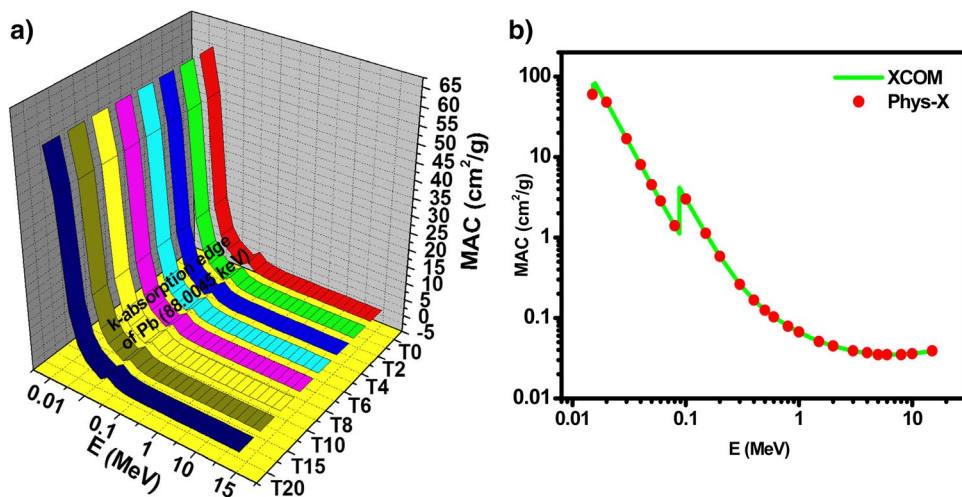
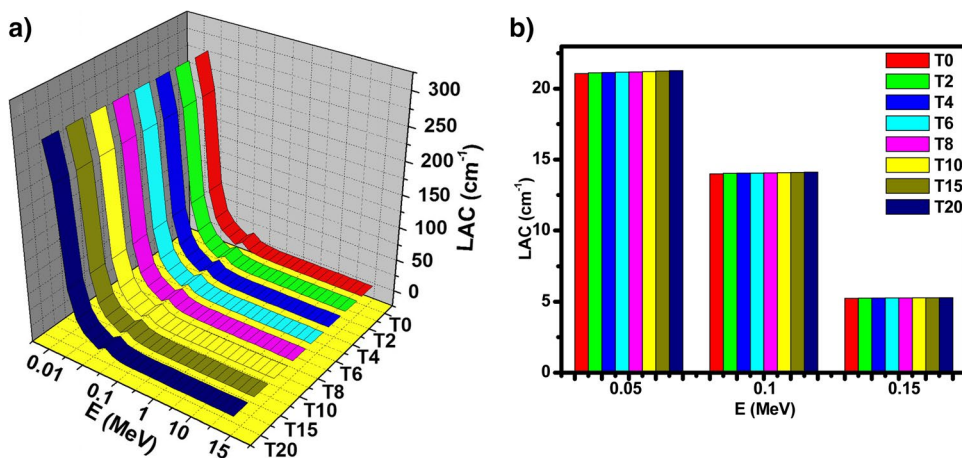


Fig. 4 **a** LAC as a function of incoming photon energy. **b** A comparison of the LAC values at selected incoming photon energies

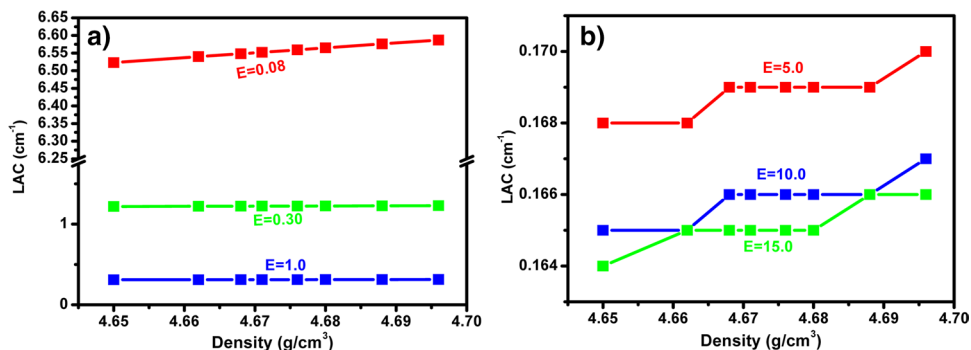


by an enhancement in the mole% of TiO_2 sub-molecular unit structures at the outlay of the evolution of the other molecular units in the molecular structure. Figure 3b shows an excellent agreement between the XCOM and Phys-X programs results approximately at the k-absorption-edge of Pb for the calculated MAC values.

The linear-attenuation coefficient (LAC) is illustrated as a three-dimensional illustration in Fig. 4a as a role of

(E). At the least incoming E, LAC values are as follows: 279.090, 279.893, 280.337, 280.601, 280.985, 281.309, 281.999, and 282.690 cm^{-1} for the sample T0, T2, T4, T6, T8, T15, and T20, respectively. Sample T20 has the highest LAC values since it has the greatest denser sample among them, but has the smallest molar volume and B_2O_3 molar content (see Fig. 4b). The internal caging structure of $30\text{Pb} + 4\text{MoO}_3 + (66-x)\text{B}_2\text{O}_3 + x\text{TiO}_2$ can be seen as

Fig. 5 The linear mass attenuation coefficient at selected incoming photon energy: **a** 0.08, 0.30, and 1.0 MeV and **b** 5.0, 8.0, 10.0, and 15.0 MeV



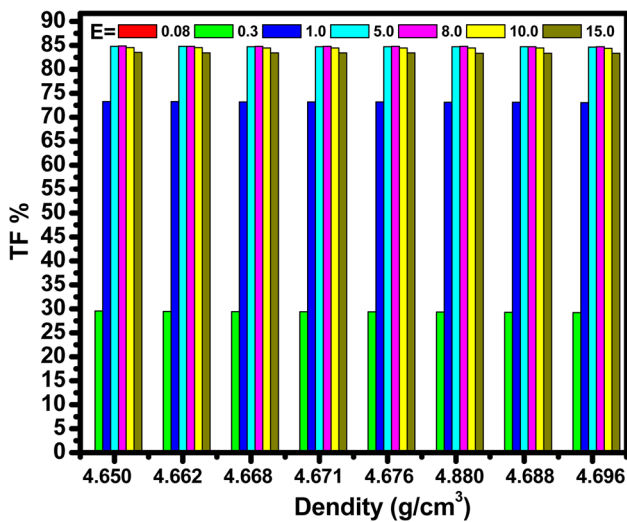


Fig. 6 The TF% as a function of density at selected incoming photon energy (in MeV) at sample’s thickness $x = 1.0$ cm

physical encasing and instantaneous trap of the γ -rays beam as follows: The existing glass systems of the various composite kinds and compression moduli can be shown in Table 2, which suggests that this type of high energetic rays is a scattering protecting process. Therefore, for such type of structural materials, the transmission coefficient (i.e., TF %) diminished as the vertex-angle in molecular packing structures is also reduced in agreement with the calculated elastic moduli (see below). The sample’s density effects on the LAC behavior may be also inferred at selected incoming energies (see Fig. 5). Our data demonstrates that this coefficient gained values are smaller than 6.5 cm^{-1} for low energies ($E = 0.08$ MeV), fewer than 0.3 cm^{-1} for intermediate energetic photons ($E = 1.0$ MeV), and much lower than 0.17 cm^{-1} for high energetic photons ($E = 1.0$ MeV). Yet, this factor’s general performance versus sample’s density maintains the similar tendency. These results have been also confirmed by Dong et al. [46] who have investigated the effect of adding oxides of the form where A_nO_m (e.g., $Nb_2O_5 = 0.01, 5$; $Nd_2O_3 = 3, 5$; and $Er_2O_3 = 5$ mol%) into a glass system of the chemical form $80TeO_2-5TiO_2-(15-x)WO_3-xA_nO_m$ glasses. The variations of the shielding

Fig. 7 Comparison between HVL for studied samples with concrete, and two RS-glasses at: a $E = 411$ keV and b $E = 1010$ keV

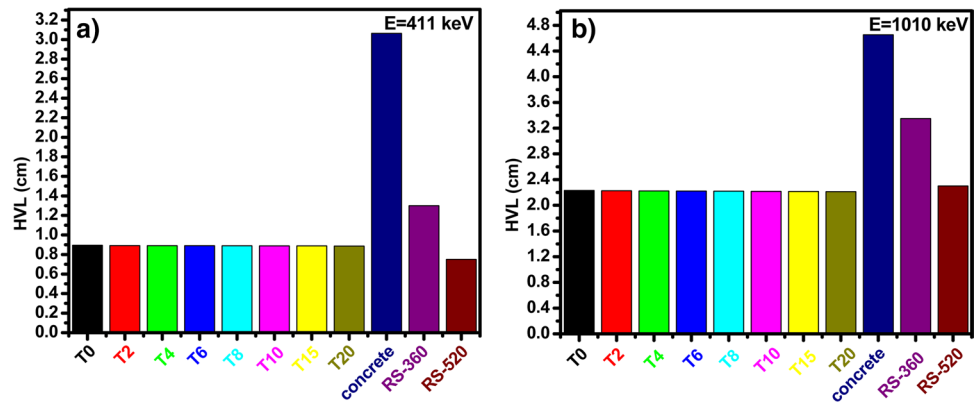
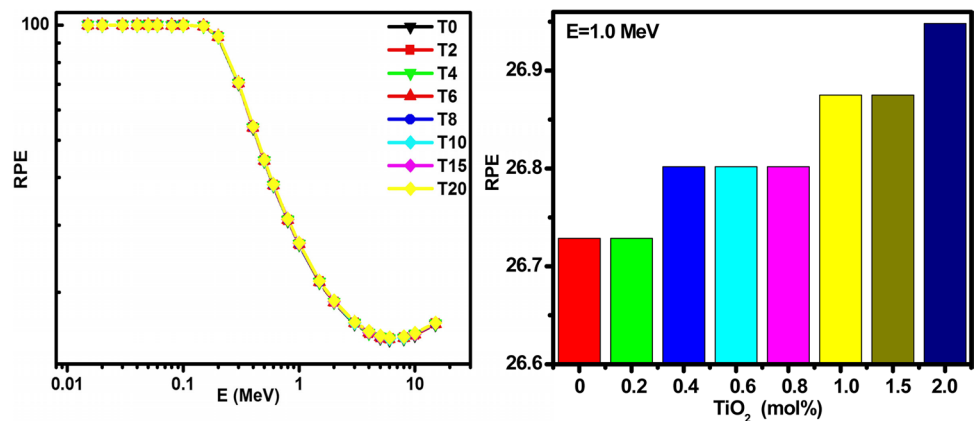


Fig. 8 The Radiation protection efficiency (RPE) for the studied samples as a function of incident photon energy (left). RPE evaluated at $E = 1.0$ MeV, the figure shows the RPE is lower for T0 (i.e., least T^{4+}) sample and greatest for T20 (i.e., greatest T^{4+}). The RPE is evaluated at sample thicknesses $x = 1.0$ cm



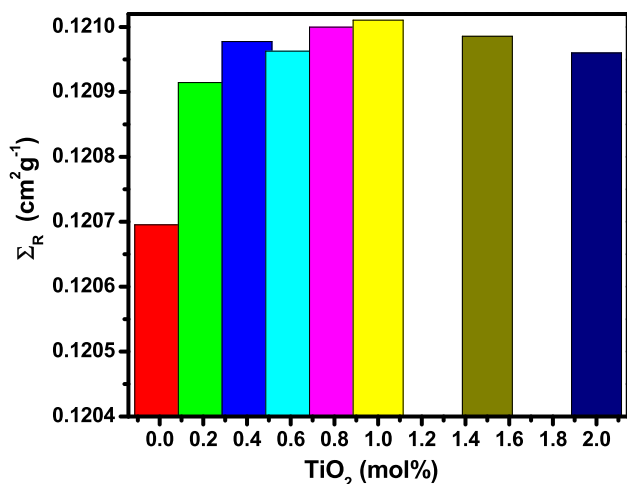


Fig. 9 The Σ_R for studied samples as a function of TiO₂ content mol%

parameters such as mass attenuation coefficients, half value layers, and macroscopic effective removal cross-section for fast neutrons have been computed by using the WinXCom program and MCNP5 Monte Carlo code. Also, the geometric progression method (G-P) was used to explore their effects on exposure buildup factor values [42]. Moreover, the effect of Fe₂O₃, TiO₂, and CdO semiconductor metal oxides was incorporated into the ZnO-MWCNT composite at different weight percentages. This group has explored the γ -ray shielding properties of these novel materials using MCNPX-Monte-Carlo-simulations. They found that at 5% oxide addition, the maximum electrical conductivity was found in all groups for all temperatures. Moreover, 5% oxide reinforcement into these glass systems resulted in maximum γ -ray attenuation properties for the CZnOCd₅ sample [43, 44]. Also, ElBatal et al. [45] investigated MoO₃-doped lithium phosphate glasses containing varying molybdenum concentrations. They combined both UV–visible and infrared (FTIR) spectroscopic to analyze these glasses before and after gamma irradiation. Their experimental findings suggested that molybdenum ions

are distributed across distinct local sites, including Mo³⁺, Mo⁴⁺, and Mo⁵⁺, in varying proportions depending on the composition of the lithium phosphate glass host and the concentration of molybdenum ions. Moreover, borophosphate glasses, with a composition of 50% P₂O₅, 30% B₂O₃, and 20% Na₂O (mol%), were prepared and subsequently measured via infrared and UV–visible absorption spectra before and after exposure to gamma irradiation. They found that the γ -irradiation produced marked changes in the UV–visible spectra of MoO₃-doped glasses. Such changes were related to the production of induced defects from photochemical reactions and the generation of positive holes. Also, they concluded that these changes are related to alternations in the bond angles and/or bond lengths of a few structural groups upon irradiation while the main structural groups remain unchanged in their number and position [30].

Figure 6 shows the TF% of the glass samples to γ -radiations as a role of density for selective photonic energies at $x=1.0$ -cm-thick blocks. This picture can be used to extract the following features. The principle of Beer-Lambert’s law is evident in the observation that the transmission of gamma rays is minimal for low-energy photons and reaches a plateau as the energy of the photons increases. Additionally, it uncovers how the glass material’s density influences these rays transmitted across an interacting media when it encounters several scattering sites on its journey through the medium. This information can be found in the work by Kavaz et al. [46]. Drawing the HVL against the sample code (TiO₂ concentration) in Fig. 7 adds to these facts. The figure demonstrates how HVL varies on sample density and input photon energy at the same time. Also, for $E=0.411$ and 1.010 MeV, the figure compares the HVL of these glasses to that of reference glass typed as RS-360 and 520. The figure unequivocally demonstrates that the TiO₂-based glasses have less effective shielding than those common materials. On the other hand, Fig. 8 shows a displacement of the radiation-defense efficacy (RPE% = 1 – TF%). For a lower-energy regime, the RPE%

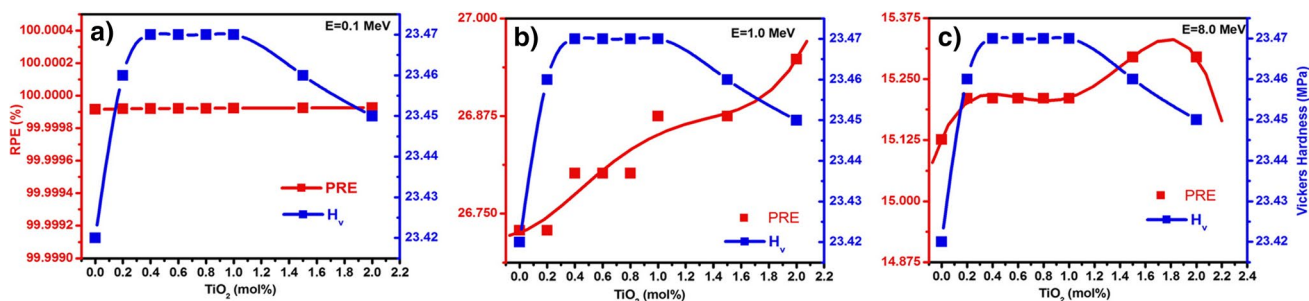


Fig. 10 A summary of the variation of the radiation protection effectiveness (RPE %) and Vickers Hardness (H_v) as a function of the sample density. The RPE is evaluated at **a** low, **b** medium, **c** high incoming photon energy. The RPE is evaluated at sample thicknesses $x=1.0$ cm

is approximately at maximum level (RPE = 100%), and the trend is then to decrease as the energy of the incoming photon increases. Because it has the smallest molar volume, sample T20 exhibits the most excellent RPE% behavior across all incoming photon spectrum energy.

For all samples in Fig. 9, the FNRCs Σ_R (cm²/g) is depicted as bars. According to the computed Σ_R of these glasses, it is found that the glass sample encoded as T10 encloses the peaked $\Sigma_R = 0.121011$ cm²/g value, indicating that the TiO₂ compound is enhancing Σ_R , thereby lessening the impact of B₂O₃. T10 also has the highest Vickers hardness value ($H_v = 23.47$ GPa), compared to other studied samples. Contrarily, the sample T0 with the lowest concentration of TiO₂ compound, which is related to the biggest molar volume, highest B₂O₃ mol% concentrations, and lowest Vickers's-hardness ($H_v = 23.42$ GPa) amid other glasses, had the lowest calculated $\Sigma_R = 0.120695$. The figure further demonstrates that when the concentration of Ti⁴⁺ ions in the sample increases, the Σ_R progressively rises and finally falls in accordance with the measured elastic moduli. Figure 10 displays the RPE%- H_v as roles as a sample's density aiming at a link between the mechano-shielding equivalents. The RPE% for low-, medium-, or high-incoming photonic ray is shown in the figure. It is obvious from this figure that the RPE%- H_v relation behaves differently depending on the incoming photon energy as a penetrating glass network. For high TiO₂ concentration, the H_v -RPE association accomplishes its greatest protection effectiveness performance. From a protection-engineering perspective, this linkage among both physically unrelated properties may pave the way for the concurrent creation of tailored glasses for particular shielding needs [30, 42–46].

Conclusion

The physical, mechano-elastic, and radiation-shielding effectiveness of various glass systems in a quarterly form $30\text{Pb} + 4\text{MoO}_3 + (66 - z)\text{B}_2\text{O}_3 + z\text{TiO}_2$, ($z \in [0.0, 2.0]$ mol%) were explored with distinctive TiO₂-based glasses. Elastic and mechanical behavior and the corresponding Poisson's-ratio showed a non-monotonic tune with TiO₂ accumulation in the glassy networks. We found that the following numerical values of the studied elastic properties, namely $20.87 < G < 22.59$ kJ/cm³, $29.60 < E < 32.07$ GPa, $0.410153 < \sigma < 0.401400$, and $0.02342 < H < 0.02345$ GPa. The inferred trend of LAC-values in the spanned energy $0.015 < E < 15.0$ has an order: $\text{LAC}_{\text{T0}} < \text{LAC}_{\text{T2}} < \text{LAC}_{\text{T4}} < \text{LAC}_{\text{T6}} < \text{LAC}_{\text{T8}} < \text{LAC}_{\text{T10}} < \text{LAC}_{\text{T15}} < \text{LAC}_{\text{T20}}$. These values ranged between $279.09 < \text{LAC} < 282.70$ cm⁻¹, at incoming photon energy of $E = 15$ keV. This highlights the communal competence

between titanium oxide and boron oxide molar fraction on the molecular structures. After being calculated, it was discovered that the Σ_R exhibits the same trending pattern as the elastic parameters. These results were also examined in terms of Ti³⁺ and Mo⁵⁺ ion sites and found that when TiO₂ exceeds 0.8 mol%, then both ions affect the studied properties via de-polymerization of the glass network. This work showed that the mechanical and shielding properties might be adjusted for scientific and/or medical purposes simultaneously.

Author contribution NAMA, ZYK, HA, YSR: conceptualization, methodology, software, validation, investigation, data creation, writing—review and editing, visualization, supervision.

Funding Princess Nourah bint Abdulrahman University Researchers Supporting Project number (PNURSP2023R60) and Princess Nourah bint Abdulrahman University, Riyadh, Saudi Arabia.

Data availability Relevant research data are included in the text of the work.

Declarations

Consent to participate Not applicable.

Consent for publication Not applicable.

Conflict of interest The authors declare no competing interests.

References

- Zumdahl, Steven S.: Chemical principles 6th Ed. Houghton Mifflin Company. p. A23. ISBN 978–0–618–94690–7 (2009)
- Völz, Hans G.; et al.: "Pigments, inorganic". Ullmann's Encyclopedia of Industrial Chemistry. Weinheim: Wiley-VCH. (2006). https://doi.org/10.1002/14356007.a20_243.pub2
- Alderman, O.L.G., Skinner, L.B., Benmore, C.J., Tamalonis, A., Weber, J.K.R.: Structure of molten titanium dioxide. *Phys. Rev. B* **90**(9), 094204 (2014)
- Emsley, John.: Nature's building blocks: an A–Z guide to the elements. Oxford: Oxford University Press. pp. 451–53. ISBN 978–0–19–850341–5 (2001)
- El, Goresy, Chen, M, Dubrovinsky, L, Gillet, P, Graup, G.: An ultradense polymorph of rutile with seven-coordinated titanium from the Ries crater. *Science*. **293**(5534), 1467–70 (2001)
- El Goresy, A., Chen, M., Gillet, P., Dubrovinsky, L., Graup, G., Ahuja, R.: A natural shock-induced dense polymorph of rutile with α -PbO₂ structure in the suevite from the Ries crater in Germany. *Earth. Planet. Sci. Lett.* **192**(4), 485 (2001)
- St. Clair, Kasia.: The secret lives of colour. London: John Murray. p. 40. ISBN 9781473630819 (2016)
- Anderson, Bruce.: Kemira pigments quality titanium dioxide. Savannah, Georgia. p. 39 (1999)
- Margaux de Frouville.: Deux dentifrices sur trois contiennent du dioxyde de titane, un colorant au possible effet cancérigène (2019)
- Koleske, J.V.: Paint and coating testing manual. ASTM International. p. 232. ISBN 978–0–8031–2060–0 (1995)

11. Mogus-Milankovic, A., Santic, A., Karabulut, M., et al.: *J. Non-cryst. Solids* **330**, 128 (2003)
12. Xu Lu, J., Chen, H., Liu, L., et al.: *Opt. Mater.* **8**, 243 (1997)
13. Syam Prasad, P., Raghavaiah, B.V., Balaji Rao, R., et al.: *Solid State. Commun.* **132**, 235 (2004)
14. Shimoji, N., Hashimoto, T., Nasu, H., et al.: *J. Non-Cryst. Solids* **324**, 50 (2003)
15. Sheik-Bahae, M., Hutchings, D.C., Hagan, D.J., et al.: *IEEE J. Quantum Electron.* **27**, 1296 (1991)
16. Koudelka, L., Mosner, P., Zeyer, M., et al.: *J. Non-Cryst. Solids* **326**, 72 (2003)
17. Murali Krishna, G., Veeraiah, N., Venkatramaiah, N. et al.: *J. Alloys Comp.* (2006)
18. Raghavaiah, B.V., Laxmikanth, C., Veeraiah, N.: *Opt. Commun.* **235**, 341 (2004)
19. da Rocha, M.S.F., Pontusuchka, W.M., Blak, A.R., Non-Cryst, J.: *Solids* **321**, 29 (2003)
20. Mogus- Milankovic, A., Santic, A., Gajovic, A., et al.: *J. Non-Cryst. Solids.* **325**, 76 (2003)
21. Ibrahim, S.E., Rammah, Y.S., Hager, I.Z., El-Mallawany, R.: UV and electrical properties of TeO₂- WO₃-Li₂O-Nb₂O₅/Sm₂O₃/Pr₆O₁₁/Er₂O₃ glasses. *J. Non-Cryst. Solids* **498**, 443–447 (2018)
22. Sayyed, M.I., El-Mallawany, R.: Shielding properties of (100-x) TeO₂-(x)MoO₃ glasses. *Mater. Chem. Phys.* **201**, 50–56 (2017)
23. Hager, I.Z., El-Mallawany, R.: Preparation and structural studied in the (70-x) TeO₂- 20WO₃-10Li₂O-xLn₂O₃ glasses. *J. Mater. Sci.* **45**, 897–905 (2010)
24. Novatski, A., Steimacher, A., Medina, A.N., Bento, A.C., Baesso, M.L., Andrade, L.H.C., Lima, S.M., Guyot, Y., Boulon, G.: Relations among nonbridging oxygen, optical properties, optical basicity, and color center formation in CaO-MgO aluminosilicate glasses. *J. Appl. Phys.* **104**, 094910–094917 (2008)
25. Moawad, H.M., Jain, H., El-Mallawany, R., Ramadan, T., El-Sharbiny, M.: Electrical conductivity of silver vanadium tellurite glasses. *J. Am. Ceram. Soc.* **85**, 2655–2659 (2002)
26. Dong, M.G., El-Mallawany, R., Sayyed, M.I., Tekin, H.O.: Shielding properties of 80TeO₂- 5TiO₂-(15-x) WO₃-xAnOm glasses using WinXCom and MCNP5 code. *Radiat. Phys. Chem.* **141**, 172–178 (2017)
27. Hager, I.Z., El-Mallawany, R., Bulou, A.: Luminescence spectra and optical properties of TeO₂- WO₃-Li₂O glasses doped with Nd, Sm and Er rare earth ion. *Phys. B* **406**, 972–980 (2011)
28. El-Mallawany, R., Sayyed, M.I., Dong, M.G., Rammah, Y.S.: Simulation of radiation shielding properties of glasses contain PbO. *Radiat. Phys. Chem.* **151**, 239–252 (2018)
29. Syam Prasad, P., Srinivasa Reddy, M., Ravi Kumar, V., Veeraiah, N.: Spectroscopic and dielectric studies on PbO-MoO₃-B₂O₃ glasses incorporating small concentrations of TiO₂. *Philos. Mag.* **87**, 5763–5787 (2007)
30. Abdelghany, A.M., Ouis, M.A., Azooz, M.A., ElBatal, H.A.: Defect formation of gamma irradiated MoO₃-doped borophosphate glasses. *Spectrochim. Acta Part A Mol. Biomol. Spectrosc.* **114**, 569–574 (2013)
31. Agostinelli, S., Allison, J., Amako, K.A., Apostolakis, J., Araujo, H., Arce, P., Asai, M., Axen, D., Banerjee, S., Barrand, G.2., Behner, F.: GEANT4—a simulation toolkit. *Nucl. Instrum. Methods Phys. Res. Sect. A Accel. Spectrom. Detect. Assoc. Equip.* **506**(3), 250–303 (2003)
32. ANSI/ANS-6.4.3 (W2001): Geometric progression gamma-ray buildup factor coefficients, American Nuclear Society, La Grange Park, Illinois (1991)
33. Berger, M.J., Hubbell, J.H.: XCOM: photon cross-sections database, Web Version 1.2 (n.d)
34. Şakar, E., Özpolat, Ö.F., Alım, B., Sayyed, M.I., Kurudirek, M.: Phy-X/PSD: development of a user friendly online software for calculation of parameters relevant to radiation shielding and dosimetry. *Radiat. Phys. Chem.* **166**, 108496 (2020)
35. Greenwood, Norman N., Earnshaw, Alan.: *Chemistry of the elements*. Oxford: Pergamon Press. pp. 1117–19. ISBN 978-0-08-022057-4 (1984)
36. Makishima, A., Mackenzie, J.D.: Direct Calculation of Young's Modulus of Glass. *J. Non-Cryst. Solids* **12**(1), 35–45 (1973)
37. Inaba, S., Fujino, S., Morinaga, K.: Young's modulus and compositional parameters of oxide glasses. *J. Am. Ceram. Soc.* **82**(12), 3501–3507 (1999)
38. Khattari, Z., Al-Buriahi, M.S.: Monte Carlo simulations and Phy-X/PSD study of radiation shielding effectiveness and elastic properties of barium zinc aluminoborosilicate glasses. *Radiat. Phys. Chem.* **195**, 110091 (2022)
39. Pauling, L.: The nature of the chemical bond and the structure of molecules and crystals 2nd ed. (Cornell University Press, Ithaca, 1940)
40. Wells, A.F.: *Structural inorganic chemistry*. Clarendon Press, Oxford (1984). (ISBN 0-19-855370-6)
41. Patnaik, Pradyot.: *Handbook of inorganic chemical compounds*. McGraw-Hill. p. 243. ISBN 0-07-049439-8 (2003)
42. Sayyed, M.I., El-Mesady, I.A., Abouhaswa, A.S., Askin, A., Rammah, Y.S.: Comprehensive study on the structural, optical, physical and gamma photon shielding features of B₂O₃-Bi₂O₃-PbO-TiO₂ glasses using WinXCOM and Geant4 code. *J. Mol. Struct.* **1197**, 656–665 (2019)
43. Dong, M.G., El-Mallawany, R., Sayyed, M.I., Tekin, H.O.: Shielding properties of 80TeO₂-5TiO₂-(15-x) WO₃-xAnOm glasses using WinXCom and MCNP5 code. *Radiat. Phys. Chem.* **141**, 172–178 (2017)
44. Basgoz, O., Guler, O., Evin, E., Yavuz, C., AlMisned, G., Issa, S.A.M., Zakaly, M.H.H., Tekin, H.O.: Synthesis and structural, electrical, optical, and gamma-ray attenuation properties of ZnO-multi-walled carbon nanotubes (MWCNT) composite separately incorporated with CdO, TiO₂, and Fe₂O₃. *Ceram. Int.* **48**, 16251–16262 (2022)
45. ElBatal, F.H., Abdelghany, A.M., Elwan, R.L.: Structural characterization of gamma irradiated lithium phosphate glasses containing variable amounts of molybdenum. *J. Mol. Struct.* **1000**, 103–108 (2011)
46. Kavaz, E., Tekin, H.O., Kilic, G., Susoy, G.: Newly developed Zinc-Tellurite glass system: an experimental investigation on impact of Ta₂O₅ on nuclear radiation shielding ability. *J. Non-Cryst. Solids* **544**, 120169 (2020)

Publisher's Note Springer Nature remains neutral with regard to jurisdictional claims in published maps and institutional affiliations.

The authors declare that this manuscript is original, has not been published before, and is not currently being considered for publication elsewhere.

Springer Nature or its licensor (e.g. a society or other partner) holds exclusive rights to this article under a publishing agreement with the author(s) or other rightsholder(s); author self-archiving of the accepted manuscript version of this article is solely governed by the terms of such publishing agreement and applicable law.